

# Enhanced permselective separation of per-fluorooctanoic acid in graphene oxide membranes by a simple PEI modification

## Supplementary Information

Sally El Meragawi<sup>†§</sup>, Abozar Akbari<sup>§#‡</sup>, Sebastian Hernandez<sup>§</sup>, Meysam Sharifzadeh  
Mirshekarloo<sup>§</sup>, Dibakar Bhattacharyya<sup>‡</sup>, Akshat Tanksale<sup>†</sup>, Mainak Majumder<sup>†§#\*</sup>

<sup>†</sup>Department of Chemical Engineering, Monash University, Clayton, VIC 3800, Australia

<sup>§</sup>Nanoscale Science and Engineering Laboratory (NSEL), Department of Mechanical and Aerospace Engineering, Monash University, Clayton, VIC 3800, Australia

<sup>‡</sup> Department of Chemical and Materials Engineering, University of Kentucky, Lexington, 40506, Kentucky, USA

<sup>‡</sup>Nematiq Pty Ltd., 2/21 Howleys Rd, Notting Hill, VIC 3168

<sup>#</sup>ARC Research Hub for Graphene Enabled Industry Transformation, Monash University, Clayton, VIC 3800, Australia

\*Corresponding Author E-mail: [mainak.majumder@monash.edu](mailto:mainak.majumder@monash.edu)

## 1. Chemical details of perfluorooctanoic acid

**Table S1.** Structure and chemical properties of perfluorooctanoic acid<sup>1-4</sup>

Compound name	Perfluorooctanoic acid
Abbreviation	PFOA
Molar mass	414 g/mol
Solubility	9.5 g/L
Micellisation concentration	3.4 g/L
pKa	-0.2
Structure	

## 2. Further characterisation

The influence of different PEI treatment times on the presence of functional groups within a laminar GO structure was evaluated through FTIR characterisation. GO films were coated by submerging them in 1 % by weight, 600 g/mol PEI for times ranging between 5 seconds and 1 minute. The GO spectrum contains a broad peak from 3000 to 3600  $\text{cm}^{-1}$  characteristic of -OH bonds in tertiary alcohols or intercalated water molecules. In the GO-PEI spectra, there are additional peaks at 3154  $\text{cm}^{-1}$  and 2815  $\text{cm}^{-1}$  which have been linked to the asymmetric and symmetric stretching of -NH and -CH<sub>2</sub> groups present in the PEI layer.<sup>5</sup> The stretching of carbonyls (-C=O) of a carboxylic acid group, the bending of -OH bonds, and the stretching of epoxide rings generate peaks at 1730  $\text{cm}^{-1}$ , 1614  $\text{cm}^{-1}$  and 1242  $\text{cm}^{-1}$ , respectively. While these peaks are all present at lower intensities in GO-PEI films compared to unmodified GO films, treatment times between 5 and 60 seconds do not cause large variations in the occurrence of these functional groups (Figure S1a). The influence of coating time on water permeance of the membrane was further evaluated and demonstrated in Figure S1b. All coating times demonstrate an improvement of water permeance compared to GO (coating time at 0 s) due to the benefits of the removal of oxygen functional groups in the GO layer and the addition of a hydrophilic top-surface coating which allows for improved nanochannel entry effects. As the coating time increases, the water permeance decreases indicating that the hydraulic resistance of the PEI layer increases either the result of an increase in the layer thickness or density. As such, for the purposes of this work, the short treatment period of 10 seconds was selected.

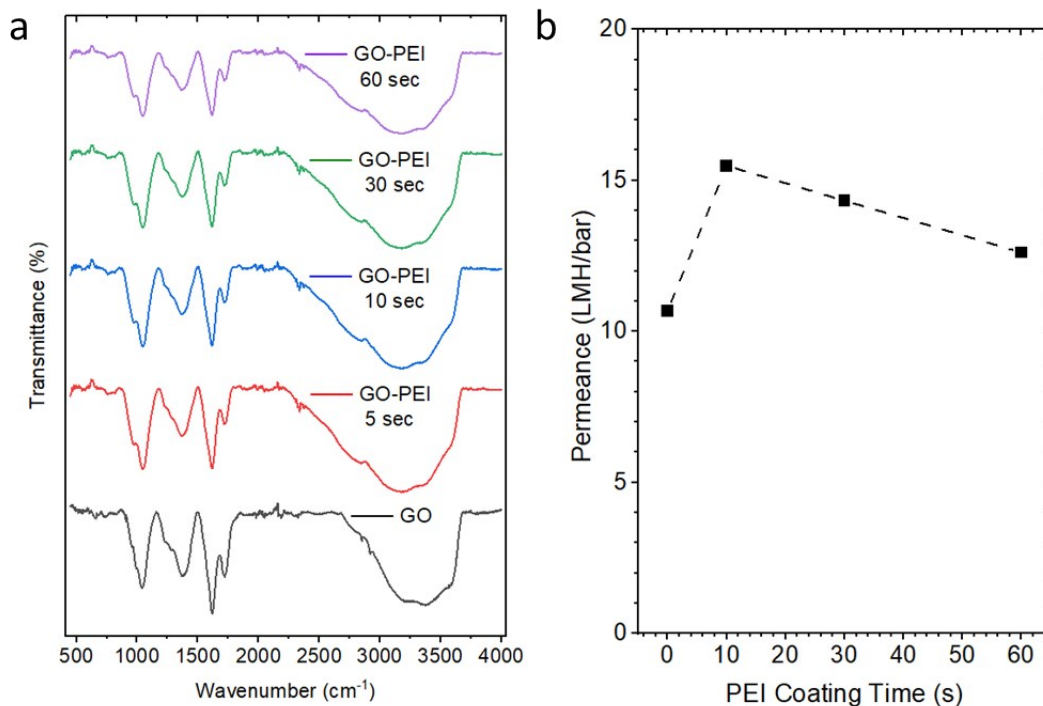


**Figure S1.** (a) FTIR of GO membranes GO and GO treated with 1 % by weight, 600 g/mol PEI for 5 to 60 seconds. (b) Water permeance of GO membranes coated in PEI for times ranging from 0 (as prepared GO membranes) to 60 s.

Analysis of the deconvoluted C1s spectra of GO (Figure S2) exhibit the expected peaks at 284.6 eV representative of C-C, C=C and C-H bonds. Two additional peaks are present at 286.2 eV, and 287.7 eV which are characteristic of -C-O and -C=O bonds, respectively. Interestingly, there is a shift in the -C=O peak to 287.3 eV, following the treatment with PEI, indicative that a proportion of the carboxylic bonds have formed covalent bonds with the amine groups present in the PEI.<sup>6</sup>

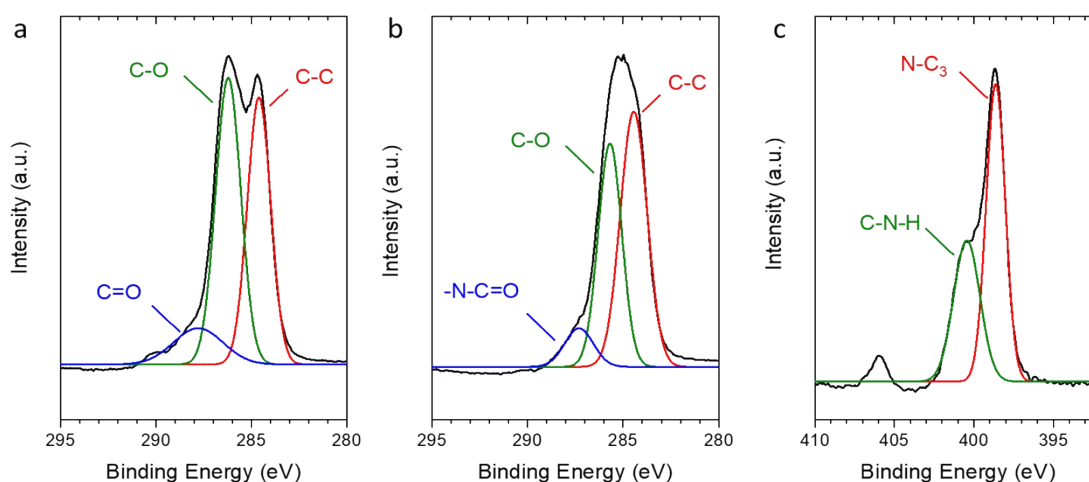


**Figure S2.** Deconvoluted C1s spectra for (a) GO and (b) GO-PEI and (c) deconvoluted N1s spectra for GO-PEI

Through XPS depth profiling, Figure S3, initially both the atomic % of nitrogen and carbon are initially constant. Following  $\sim 5$  mins of etching, the nitrogen content begins to decrease while the carbon content increases. In the initial region where the nitrogen and carbon content of the GO-PEI membrane is constant, most of the signal is coming from PEI. Indicating that PEI occurs primarily on the top surface of the membrane. With further etching, sampling of the GO-PEI interface and later GO occurs. With increasing etching, the nitrogen content of the GO layer does not fall to negligible levels, indicating that some diffusion of PEI into GO layer may have occurred.

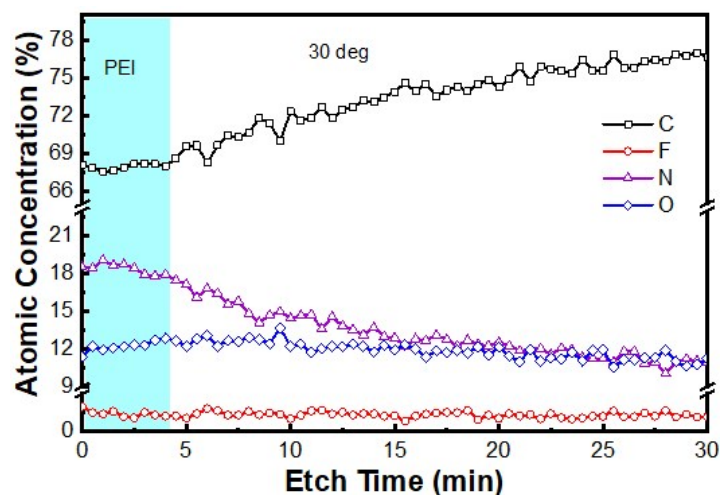


**Figure S3.** XPS Depth profiling of a GO-PEI membrane highlighting the change in atomic concentration over the width of the sample as indicated by the etch time.

Remarkably, the presence of this PEI film has the added benefit of increasing the abrasion resistance of the GO membrane in wet conditions. The abrasive resistance of the membrane was characterised using a BYK-Gardner wet abrasion scrub tester; abrasion scrub testing involved wetting the membranes with DI water and cycling an abrasive sponge in a reciprocating linear motion until delamination of the film is observed. Wet abrasion scrubbing resistance tests are widely used in the detaching of paints from surfaces.<sup>7</sup> A GO membrane completely delaminated after only 10 cycles (Figure S4a) while a GO-PEI membrane was uncompromised after 52 cycles (Figure S4b) and only began to show damage similar to that of the GO membrane around 200 cycles. PEI has previously been shown to improve the adhesion between a tannic acid film and a PVDF membrane as a result of the stability of the crosslinked network.<sup>8</sup> The improved mechanical stability is derived from the reduced mobility of the graphene oxide sheets covalently bound to the PEI layer and the potential occurrence of interstitial crosslinking in the top surface layers of the membrane.<sup>9</sup> This improved mechanical stability indicates that this modification may improve the long-term stability of the membrane during filtration.

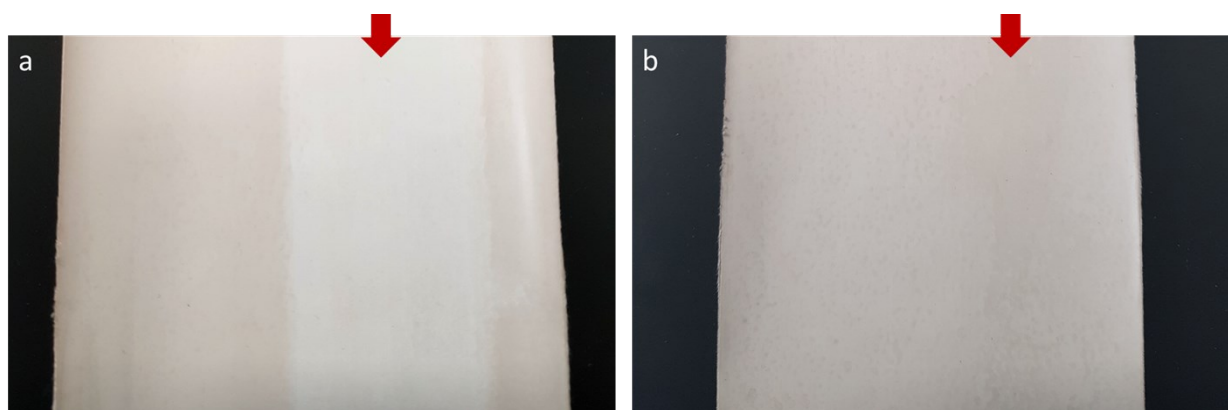


**Figure S4.** Photographs of (a) GO membrane after 10 cycles and (b) GO-PEI membrane after 50 cycles following abrasion resistance scrubbing. Red arrows indicate area of abrasion testing.

The influence of charge exclusion by both the GO and GO-PEI membranes was evaluated through salt retention tests. In particular, the ability of GO and GO-PEI films to retain NaCl, Na<sub>2</sub>SO<sub>4</sub>, MgCl<sub>2</sub> and CaCl<sub>2</sub> salt was evaluated. Salt retention was determined through dead-end characterisation where 80 mL of a 100 mL, pH of 7, 25 mM feed was permeated through a GO membrane and a GO-PEI membrane at 1 bar. PEI modification resulted in a drop in salt retention to  $9.2 \pm 1.1$  % from the  $14.9 \pm 2.5$  % of GO membranes. Similarly, the retention of Na<sub>2</sub>SO<sub>4</sub> drops from  $31.1 \pm 1.1$  % to  $11.6 \pm 0.79$  % following PEI functionalisation. This

decreased retention, shown in Figure S5, further reflects the removal of negative charges from the GO during PEI treatment. Conversely, the retention of  $\text{CaCl}_2$  by a GO membrane increases from  $11.9 \pm 1.9 \%$  to  $19.4 \pm 1.9 \%$  following PEI treatment. This is reflective of the presence of the positively charged amine groups in the PEI layer.

The salt retention sequence for the GO membrane is  $R(\text{Na}_2\text{SO}_4) > R(\text{NaCl}) > R(\text{CaCl}_2) > R(\text{MgCl}_2)$ . This sequence can be explained by Donnan exclusion theory and hydration radius impact which describes the retention of charges by a charged nanofiltration membrane.<sup>10</sup> To maintain the electroneutrality of the permeate and retentate streams during membrane filtration as co-ions are excluded so are the counter-ions.<sup>11</sup> Thus, the retention of salts is dependent on the valences of the cations and anions present in the solution. Charge-based retention of asymmetric salts, such as  $\text{MgCl}_2$ ,  $\text{CaCl}_2$  and  $\text{Na}_2\text{SO}_4$ , is governed by the retention of the higher valency ions due to the electrostatic interactions between the ions and the membrane.<sup>12</sup> Consequently, the retention of  $\text{MgCl}_2$  or  $\text{CaCl}_2$  by the negatively charged GO membranes is mainly controlled by the permeation of the  $\text{Mg}^{2+}$  or  $\text{Ca}^{2+}$  ions while the retention of  $\text{Na}_2\text{SO}_4$  is controlled by  $\text{SO}_4^{2-}$ . For a negatively charged membrane this results in the retention order described previously. The modification of the GO membrane with PEI introduces positive charge centres to the membrane which increases the retention of the high valence cations and decreases the retention of the anions resulting in the retention order observed in Figure S5 for GO-PEI membranes.

Overall, the low retention of these salts combined with the high retention of PFOA establishes this membrane as a loose nanofiltration membrane.<sup>13</sup> In comparison, membranes capable of retaining PFAS such as the piperazine and NF270 membranes fabricated and tested by Boo et al exhibit a concomitant high salt retention.<sup>14</sup> They demonstrated that these membranes with retentions of over 90% for PFOA had retentions of  $> 40 \%$  for  $\text{CaCl}_2$ ,  $> 70 \%$  for  $\text{NaCl}$ , and  $\sim 100 \%$  for  $\text{Na}_2\text{SO}_4$ .<sup>14</sup> In comparison, the membranes fabricated in this work have  $< 35 \%$  retention for all salt species. This low retention of salts indicates that the influence of electrostatic (Donnan) exclusion is not a significant mechanism in the retention of charged solutes by GO and GO-PEI membranes.

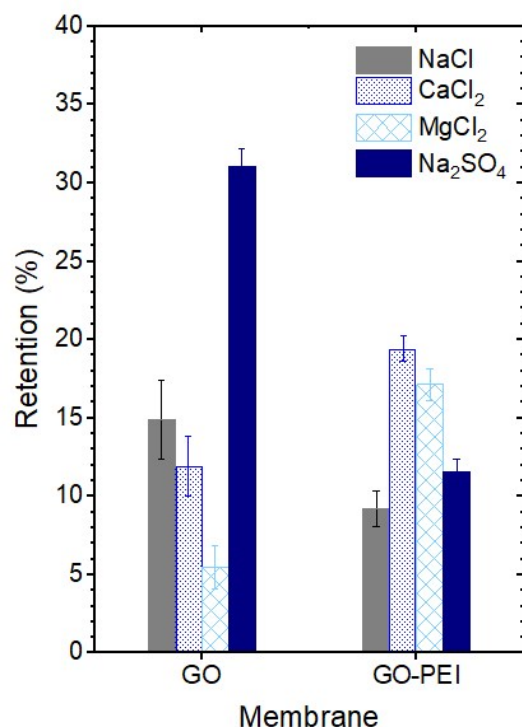


**Figure S5.** Retention of 25 mM NaCl, CaCl<sub>2</sub>, MgCl<sub>2</sub>, and Na<sub>2</sub>SO<sub>4</sub> by GO and GO-PEI membranes

The retention of differently charged dye probes across a range of molecular weights were tested to evaluate the molecular weight cut-off (MWCO) of the GO and modified GO-PEI membranes. Here, 80 mL was permeated from a 100 mL feed concentrated at 30 mg/L. The GO-PEI membranes showed high retention (> 98 %) for negatively charged species with molecular weight above 400 Da while GO membranes exhibit a lower retention (> 90 %). For positively charged species with molecular weights below 350 Da (such as Methylene blue with a MW of 319.9 Da), GO-PEI membranes with a retention of  $81.7 \pm 4.5$  % outperformed GO membranes ( $70.1 \pm 4.1$ %) by over a 10% margin. For neutral probes (Methyl red), GO-PEI membranes have a higher retention compared to GO membranes.

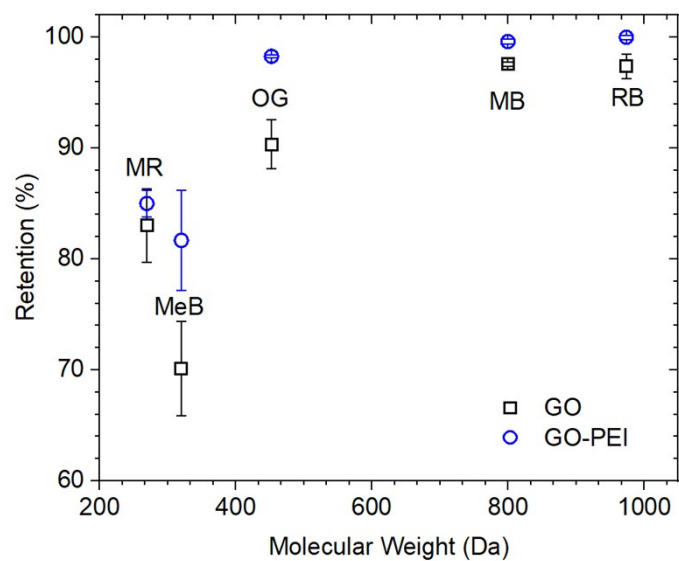


**Figure S6.** Retention performance as a function of molecular weight for probe molecules with different charges and sizes for GO (black square) and GO-PEI (blue circle) membranes. The negatively charged probes are Rose Bengal (RB), Methyl Blue (MB), and Orange G (OG), the positively charged probe is Methylene blue (MeB), and the neutrally charged probe is Methyl Red (MR).

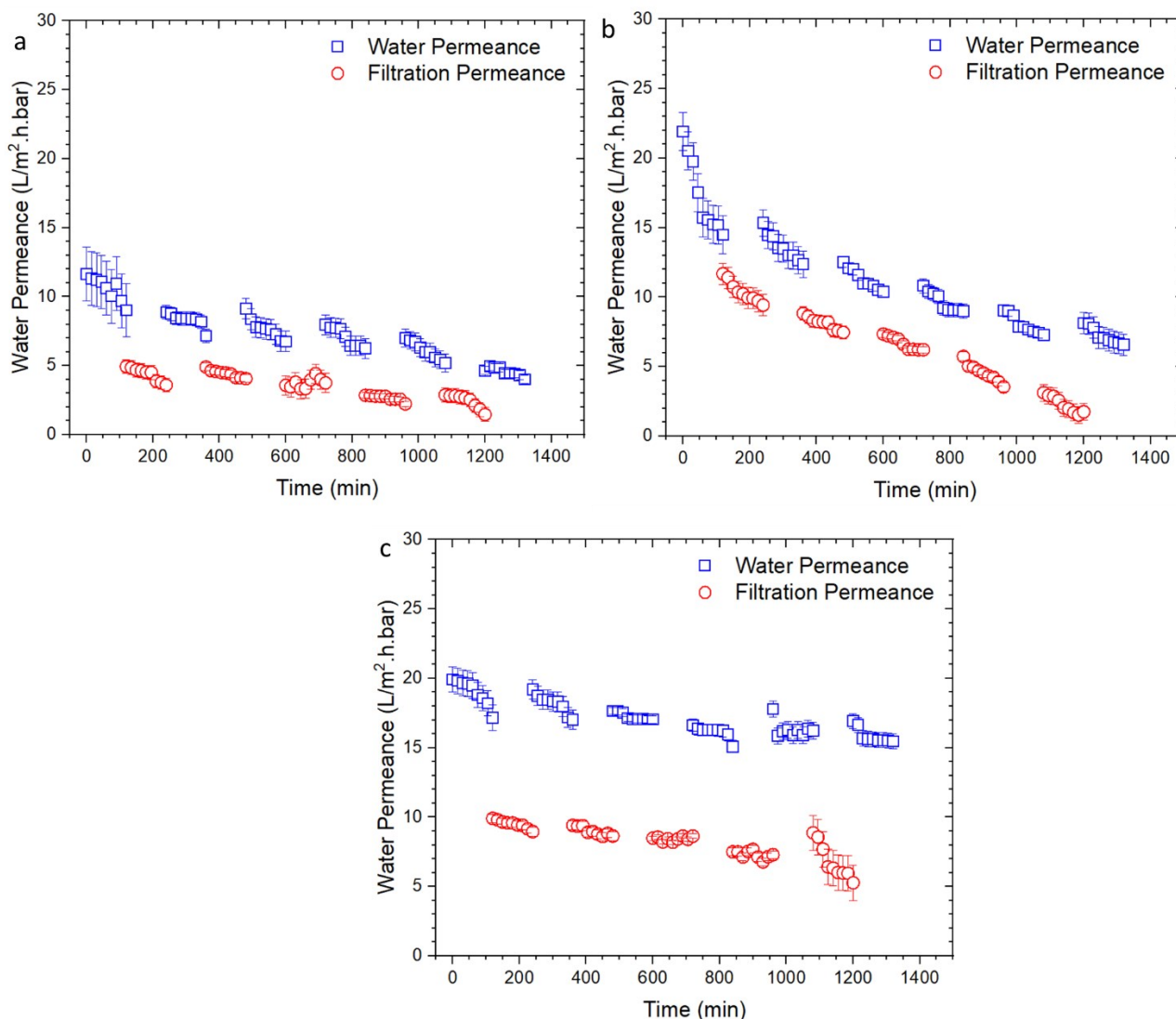


**Figure S7.** BSA Fouling of (a) GO membrane with Ethanol cleaning, (b) GO-PEI membrane with Ethanol Cleaning, and (c) GO-PEI membrane with sodium hydroxide cleaning.

GO and GO-PEI membranes were fouled with Bovine serum albumin (BSA) and cleaned with ethanol (absolute) and sodium hydroxide (pH of 9). Initially, water permeance of the clean membrane was recorded. Then, an iterative fouling/cleaning procedure was used to test the improvement of the PEI modification on the anti-fouling property of the membrane and was implemented in three steps: (i) fouling, (ii) washing and chemical cleaning, followed by (iii) water filtration. This iterative process was repeated 5 times per membrane sample.

In the first step, a GO membrane was fouled by filtering 30 mg/L BSA solution through a GO (Figure S7a) or GO-PEI (Figure S7b-c) for 2 hours in a dead-end cell. Next, to wash the membrane 50 mL of a cleaning solution (ethanol or sodium hydroxide at pH of 9) was stirred at 800 rpm for 5 minutes. Then, a fresh feed of cleaning solution was filtered through the

membrane for 15 minutes. Finally, DI water was permeated through the membrane for 2 hours to rinse the membrane from any residual cleaning solution, and measure recovered water permeance. Similar protocols have been described elsewhere.<sup>15-17</sup>

The anti-fouling potential may be evaluated by flux recovery (FR) which may be calculated as per Eq.1:

$$FR = \frac{J_{w,f}}{J_{w,1}} \times 100\% \quad \text{Eq. 1}$$

Where,  $J_{w,1}$  is the initial DI water permeance of the membrane before the first cycle and,  $J_{w,f}$  is the membranes water permeance for the final cycle.

In cleaning the GO membrane with ethanol, a flux recovery of 50% was obtained (Figure S7a). In comparison, for GO-PEI membranes fouled with BSA and cleaned with ethanol the flux recovery was 56% (Figure S7b). This change can be attributed to the increase in the hydrophilic character of the GO-PEI membrane (as per contact angle characterisation). Hydrophilicity is a key membrane property in enhancing the anti-fouling property of a membrane.<sup>18</sup> This is because an increase in the preference for water molecules to adsorb to the membrane surface enhances the hydration forces between the membrane and BSA and reducing membrane fouling.<sup>19,20</sup> The use of sodium hydroxide as a cleaning agent had a higher cleaning efficiency with a flux recovery of 98% (Figure S7c). The use of a high pH cleaning solution results in the deprotonation of the functional groups on the GO and increases the dissolution of BSA from the membrane surface.<sup>21</sup>

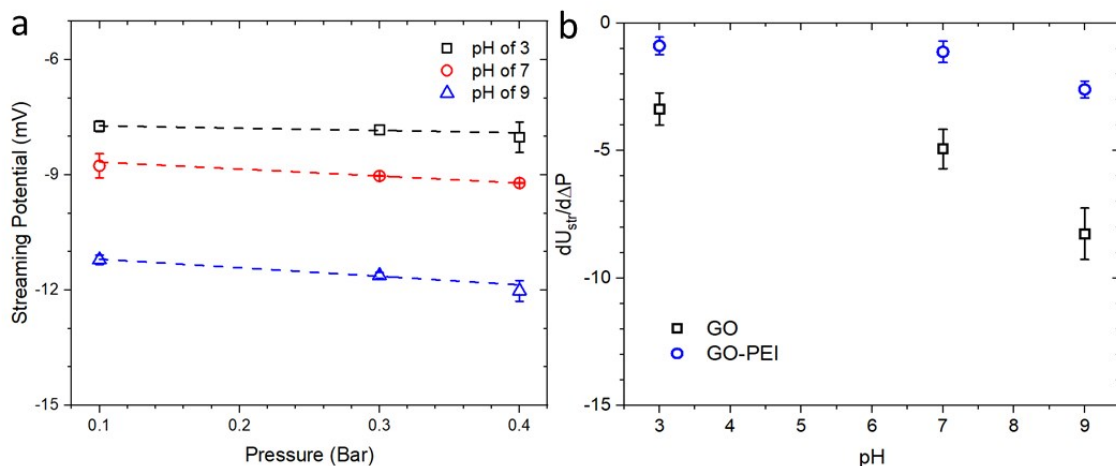


**Figure S8.** (a) Streaming potential of a GO-PEI membranes and (b) change in streaming potential with applied pressure across pHs ranging from acidic to basic for GO (black squares) and GO-PEI (blue circles) membranes.

To investigate the streaming potential, a membrane sample was placed in a nanofluidic cell bracketed by reservoirs containing 1 g/L KCl solution as an electrolyte and silver/silver chloride electrodes for electrical current measurements. Pressures varying between 100 and 400 mbar were applied via a Fluigent pressure pump (MFCS-EX Extended flow control, France) and voltage response was measured on a Keithley 6403 source measurement unit. The change in streaming potential measurements of GO and GO-PEI membranes with applied pressure at different pHs (3-9) are shown in Figure S8.

The application of a pressure differential ( $\Delta P$ ) across membrane, the flow of the electrolyte through the membrane causes a charge separation which yields a streaming potential ( $dU_{str}$ ) that is proportional to the zeta potential ( $\zeta$ ), the free-space permittivity ( $\epsilon^0$ ), and the dielectric coefficient of the electrolyte ( $\epsilon$ ). The streaming potential also inversely varies with the electrolyte viscosity ( $\eta$ ) and the electrolyte conductivity ( $\kappa_B$ ) as described through the Helmholtz–Smoluchowski model as per Eq. 2.<sup>22</sup>

$$\zeta = \frac{dU_{str}}{d\Delta P} \times \frac{\eta}{\epsilon \cdot \epsilon_0} \times \kappa_B \quad \text{Eq. 2}$$

The streaming potential allows for the characterisation of the magnitude and sign of the effective surface charge associated with the double layer at the membrane surface and thus provides a measure of the increase in ionised functional groups at different conditions.<sup>23</sup> For GO membranes at acidic pHs, a majority of the functional groups are deionised and the zeta potential is low in magnitude. As the pH increase, more groups become ionised and the

potential drops. Following modification with PEI, the potential, hence the surface charge, of the membrane is changed across the entire pH range as a result of the PEI modification. Furthermore, for GO-PEI membranes the change in the zeta potential with pH is far less pronounced indicating that surface charge changes have a smaller impact on the retention mechanism of the membrane compared to GO membranes.

### 3. Summary of PFAS treatment technologies

**Table S2.** Current state of treatment technologies for the remediation of PFAS contaminated water.<sup>14,24-43</sup>

Treatment	PFAS chemical	Water source	PFAS influent conc.	Percent removal	Flow rate	Reference
<b>Photocatalysis</b>						
254 nm UV + TiO <sub>2</sub>	PFOA	Lab prepared samples	50 mg/L	15%	N/A	Chen 2015 <sup>28</sup>
254 nm UV + TiO <sub>2</sub> -Cu	PFOA	Lab prepared samples	50 mg/L	80%	N/A	Chen 2015 <sup>28</sup>
254 nm UV + TiO <sub>2</sub> -Fe	PFOA	Lab prepared samples	50 mg/L	60%	N/A	Chen 2015 <sup>28</sup>
365 nm UV + TiO <sub>2</sub> -Pd	PFOA	Lab prepared samples	60 mg/L	98%	N/A	Li 2016 <sup>24</sup>
254 nm UV + Ga <sub>2</sub> O <sub>3</sub>	PFOA	Lab prepared samples	40 mg/L	40%	N/A	Zhao 2009 <sup>25</sup>
254 nm UV + In <sub>2</sub> O <sub>3</sub>	PFOA	Lab prepared samples	80 µmol/L	75%	N/A	Li 2012 <sup>26</sup>
254 nm UV + In <sub>2</sub> O <sub>3</sub> -CeO <sub>2</sub>	PFOA	Lab prepared samples	100 mg/L	100%	N/A	Jiang 2016 <sup>27</sup>
<b>Other destructive PFAS treatment processes</b>						
Heat-activated persulfate oxidation	PFOA	Lab prepared samples	155 mg/L	77.5%	N/A	Hori 2008 <sup>29</sup>
Subcritical water+iron oxidation	PFOS	Lab prepared samples	186 mg/L	97.6%	N/A	Hori 2008 <sup>29</sup>
Thermal treatment at 950 °C	PFOA	Lab prepared samples	16 g/L	99%	N/A	Yamada 2005 <sup>30</sup>
Sonolysis	PFOA	Aqueous dilution of FC-600	161 mg/L	40%	N/A	Vecitis 2010 <sup>31</sup>
<b>Activated carbon (Granular (GAC) and Powdered (PAC))</b>						
GAC (Norit GAC300)	PFOS	River water	2.3 ng/L	89%	5 mgpd	Appleman 2014 <sup>32</sup>
GAC (Norit GAC300)	PFOA	River water	9.7 ng/L	48%	5 mgpd	Appleman 2014 <sup>32</sup>
<b>Activated carbon cont.</b>						
GAC (Filtrisorb 400 Calgon Carbon)	PFOA	Spiked drinking water	66-116 ng/L	64%	36 mL/min	McCleaf 2017 <sup>33</sup>

GAC (Filtrisorb 400 Calgon Carbon)	PFOS	Spiked drinking water	28-62 ng/L	71-81%	36 mL/min	McCleaf 2017 <sup>33</sup>
GAC (bituminous coal)	PFOA	Spiked drinking water	0.92 µg/L	75-80%	8.4 mL/min	McNamara 2018 <sup>34</sup>
PAC	PFOA	Groundwater	550 ng/L	68%	N/A	Pramanik 2015 <sup>35</sup>
GAC (Filtrisorb 400 Calgon Carbon)	PFOA	Groundwater	10 ng/L	38%	75 mL/min	Franke 2019 <sup>36</sup>
<b>Anionic Exchange</b>						
AIX (Purolite FerrIX A33)	PFOS	Groundwater	2.6-4.5 ng/L	90-94%	350 gpm	Appleman 2014 <sup>32</sup>
AIX (Purolite FerrIX A33)	PFOA	Groundwater	68-120 ng/L	73-76%	350 gpm	Appleman 2014 <sup>32</sup>
IEX (Sorbix A3F resin)	PFOS	Groundwater	4.2-32 µg/L	99%	3.6 gpm	Woodard 2017 <sup>34</sup>
IEX (Sorbix A3F resin)	PFOA	Groundwater	9.1-13 µg/L	99%	3.6 gpm	Woodard 2017 <sup>34</sup>
AIX (Purolite A-600)	PFOA	Spiked drinking water	66-116 ng/L	65%	36 mL/min	McCleaf 2017 <sup>33</sup>
AIX (Purolite A-600)	PFOS	Spiked drinking water	28-62 ng/L	96%	36 mL/min	McCleaf 2017 <sup>33</sup>
<b>Membrane filtration</b>						
UF	PFOS	Groundwater	13-20 ng/L	0%	N/A	Atkinson et al 2008 <sup>37</sup>
UF	PFOA	wastewater	32-56 ng/L	7-51%	40 ML/d	Thompson 2011 <sup>38</sup>
NF270	PFOA	Spiked drinking water	664 ng/L	97%	4.5 mL/min	Appleman 2013 <sup>39</sup>
NF270-400 Dow filmtech	PFOA	Groundwater	10 ng/L	85%	2.3 m <sup>3</sup> /h	Franke 2019 <sup>36</sup>
NF270	PFOA	Lab prepared samples	1 mg/L	90%	9.4 LMH/bar	Boo 2018 <sup>14</sup>
NF Piperazine + Bipiperidyl dihydrochloride	PFOA	Lab prepared samples	1 mg/L	89%	8.1 LMH/bar	Boo 2018 <sup>14</sup>
<b>Membrane filtration (cont.)</b>						
NF270 (Dow FilmTec)	PFOS	Lab prepared samples	10 mg/L	83.6%	1.37 L/min	Tang 2007 <sup>40</sup>
NF DK (GE Osmonics)	PFOS	Lab prepared samples	10 mg/L	97.6%	1.37 L/min	Tang 2007 <sup>40</sup>
NF90 (Dow FilmTec)	PFOS	Lab prepared samples	10 mg/L	99.1%	1.37 L/min	Tang 2007 <sup>40</sup>

Reduced Graphene Oxide	PFOA	Lab prepared samples	1 mg/L	72%		Aher 2020 <sup>41</sup>
Membrane filtration plant, Japan	PFOA	River water	5.2 -32 ng/L	25-55%	N/A	Takagi et al. 2008 <sup>42</sup>
RO	PFOA	Wastewater	15 ng/L	66%	N/A	Quinones 2009 <sup>43</sup>
RO (polyamide ESPA2 Hydranautics)	PFOS	wastewater	3-14 ng/L	96-99%	12 gsf	Appleman 2014 <sup>32</sup>
RO (polyamide ESPA2 Hydranautics)	PFOA	wastewater	11-160 ng/L	47-98%	12 gsf	Appleman 2014 <sup>32</sup>
RO	PFOA	wastewater	21-52 ng/L	93-97%	40 ML/d	Thompson 2011 <sup>38</sup>
RO (ESPA3 Hydranautics)	PFOS	Lab prepared samples	10 mg/L	98.5	1.37 L/min	Tang 2007 <sup>40</sup>
RO (LFC1 Hydranautics)	PFOS	Lab prepared samples	10 mg/L	99.8	1.37 L/min	Tang 2007 <sup>40</sup>
RO (BW30 Dow FilmTec)	PFOS	Lab prepared samples	10 mg/L	99.8	1.37 L/min	Tang 2007 <sup>40</sup>
<b>Performance of membranes developed in this work</b>						
Graphene Oxide	PFOA	Lab prepared samples	50 mg/L	64.1%	3.3 LMH/bar	This work
Graphene Oxide	PFOA	Lab prepared samples	100 mg/L	51.5%	2.6 LMH/bar	This work
Graphene Oxide	PFOA	Lab prepared samples	200 mg/L	15.9%	1.8 LMH/bar	This work
Graphene Oxide-Polyethyleneimine	PFOA	Lab prepared samples	50 mg/L	93.7%	12.6 LMH/bar	This work
Graphene Oxide-Polyethyleneimine	PFOA	Lab prepared samples	100 mg/L	92.9%	10.9 LMH/bar	This work
Graphene Oxide-Polyethyleneimine	PFOA	Lab prepared samples	200 mg/L	79.6%	8.9 LMH/bar	This work

#### 4. References

- (1) Flores, C.; Ventura, F.; Martin-Alonso, J.; Caixach, J. Occurrence of Perfluorooctane Sulfonate (PFOS) and Perfluorooctanoate (PFOA) in N.E. Spanish Surface Waters and Their Removal in a Drinking Water Treatment Plant That Combines Conventional and Advanced Treatments in Parallel Lines. *Sci. Total Environ.* **2013**, *461–462*, 618–626.
- (2) Rahman, M. F.; Peldszus, S.; Anderson, W. B. Behaviour and Fate of Perfluoroalkyl and Polyfluoroalkyl Substances (PFASs) in Drinking Water Treatment: A Review. *Water Res.* **2014**, *50*, 318–340.
- (3) Zhao, L.; Bian, J.; Zhang, Y.; Zhu, L.; Liu, Z. Comparison of the Sorption Behaviors and Mechanisms of Perfluorosulfonates and Perfluorocarboxylic Acids on Three Kinds of Clay Minerals. *Chemosphere* **2014**, *114* (November 2014), 51–58.
- (4) Chen, W.; Zhang, X.; Mamadiev, M.; Wang, Z. Sorption of Perfluorooctane Sulfonate and Perfluorooctanoate on Polyacrylonitrile Fiber-Derived Activated Carbon Fibers: In Comparison with Activated Carbon. *RSC Adv.* **2017**, *7* (2), 927–938.
- (5) Zhao, R.; Kong, W.; Sun, M.; Yang, Y.; Liu, W.; Lv, M.; Song, S.; Wang, L.; Song, H.; Hao, R. Highly Stable Graphene-Based Nanocomposite (GO-PEI-Ag) with Broad-Spectrum, Long-Term Antimicrobial Activity and Antibiofilm Effects. *ACS Appl. Mater. Interfaces* **2018**, *10* (21), 17617–17629.
- (6) Roy, S.; Tang, X.; Das, T.; Zhang, L.; Li, Y.; Ting, S.; Hu, X.; Yue, C. Y. Enhanced Molecular Level Dispersion and Interface Bonding at Low Loading of Modified Graphene Oxide to Fabricate Super Nylon 12 Composites. *ACS Appl. Mater. Interfaces* **2015**, *7* (5), 3142–3151.
- (7) Wu, W.; Severtson, S.; Miller, C. Alkali-Soluble Resins (ASR) and Acrylic Blends: Influence of ASR Distribution on Latex Film and Paint Properties. *J. Coatings Technol. Res.* **2016**, *13* (4), 655–665.
- (8) Wu, L.; Lin, Q.; Liu, C.; Chen, W. A Stable Anti-Fouling Coating on PVDF Membrane Constructed of Polyphenol Tannic Acid, Polyethyleneimine and Metal Ion. *Polymers (Basel)*. **2019**, *11* (12).
- (9) Nam, Y. T.; Choi, J.; Kang, K. M.; Kim, D. W.; Jung, H. T. Enhanced Stability of Laminated Graphene Oxide Membranes for Nanofiltration via Interstitial Amide Bonding. *ACS Appl. Mater. Interfaces* **2016**, *8* (40), 27376–27382.
- (10) Bandini, S.; Vezzani, D. Nanofiltration Modeling: The Role of Dielectric Exclusion in Membrane Characterization. *Chem. Eng. Sci.* **2003**, *58* (15), 3303–3326.
- (11) Schaep, J.; Van Der Bruggen, B.; Vandecasteele, C.; Wilms, D. Influence of Ion Size and Charge in Nanofiltration. *Sep. Purif. Technol.* **1998**, *14*, 155–162.
- (12) Teixeira, M. R.; Rosa, M. J.; Nyström, M. The Role of Membrane Charge on Nanofiltration Performance. *J. Memb. Sci.* **2005**, *265* (1–2), 160–166. <https://doi.org/10.1016/j.memsci.2005.04.046>.
- (13) Schäfer, A. I.; Andritsos, N.; Anastasios, J.; Hoek, E. M. V.; Schneider, R. *Chapter 8 Fouling in Nanofiltration*; 2004.
- (14) Boo, C.; Wang, Y.; Zucker, I.; Choo, Y.; Osuji, C. O.; Elimelech, M. High Performance Nanofiltration Membrane for Effective Removal of Perfluoroalkyl

- Substances at High Water Recovery. *Environ. Sci. Technol.* **2018**, *52* (13), 7279–7288.
- (15) El Meragawi, S.; Akbari, A.; Hernandez, S.; Tanksale, A.; Majumder, M. Efficient Permeance Recovery of Organically Fouled Graphene Oxide Membranes. *ACS Appl. Bio Mater.* **2020**, *3* (1), 584–592. <https://doi.org/10.1021/acsabm.9b00975>.
  - (16) Li, Q.; Elimelech, M. Organic Fouling and Chemical Cleaning of Nanofiltration Membranes: Measurements and Mechanisms. *Environ. Sci. Technol.* **2004**, *38* (17), 4683–4693.
  - (17) Tin, M. M. M.; Anioke, G.; Nakagoe, O.; Tanabe, S.; Kodamatani, H.; Nghiem, L. D.; Fujioka, T. Membrane Fouling, Chemical Cleaning and Separation Performance Assessment of a Chlorine-Resistant Nanofiltration Membrane for Water Recycling Applications. *Sep. Purif. Technol.* **2017**, *189*, 170–175.
  - (18) Ayyaru, S.; Ahn, Y.-H. Application of Sulfonic Acid Group Functionalized Graphene Oxide to Improve Hydrophilicity, Permeability, and Antifouling of PVDF Nanocomposite Ultrafiltration Membranes. **2016**. <https://doi.org/10.1016/j.memsci.2016.10.048>.
  - (19) Miao, R.; Wang, L.; Zhu, M.; Deng, D.; Li, S.; Wang, J.; Liu, T.; Lv, Y. Effect of Hydration Forces on Protein Fouling of Ultrafiltration Membranes: The Role of Protein Charge, Hydrated Ion Species, and Membrane Hydrophilicity. *Environ. Sci. Technol.* **2017**, *51* (1), 167–174.
  - (20) Safarpour, M.; Khataee, A.; Vatanpour, V. Preparation of a Novel Polyvinylidene Fluoride (PVDF) Ultrafiltration Membrane Modified with Reduced Graphene Oxide/Titanium Dioxide (TiO<sub>2</sub>) Nanocomposite with Enhanced Hydrophilicity and Antifouling Properties. *Ind. Eng. Chem. Res.* **2014**, *53* (34), 13370–13382.
  - (21) Sohrabi, M. R.; Madaeni, S. S.; Khosravi, M.; Ghaedi, A. M. Chemical Cleaning of Reverse Osmosis and Nanofiltration Membranes Fouled by Licorice Aqueous Solutions. *DES* **2010**, *267*, 93–100. <https://doi.org/10.1016/j.desal.2010.09.011>.
  - (22) Mouterde, T.; Keerthi, A.; Poggioli, A. R.; Dar, S. A.; Siria, A.; Geim, A. K.; Bocquet, L.; Radha, B. Molecular Streaming and Its Voltage Control in Ångström-Scale Channels. *Nature* **2019**, *567* (7746), 87–90. <https://doi.org/10.1038/s41586-019-0961-5>.
  - (23) Fan, B.; Bhattacharya, A.; Bandaru, P. R. Enhanced Voltage Generation through Electrolyte Flow on Liquid-Filled Surfaces. *Nat. Commun.* **2018**, *9* (1), 1–7. <https://doi.org/10.1038/s41467-018-06297-9>.
  - (24) Li, M.; Yu, Z.; Liu, Q.; Sun, L.; Huang, W. Photocatalytic Decomposition of Perfluorooctanoic Acid by Noble Metallic Nanoparticles Modified TiO<sub>2</sub>. *Chem. Eng. J.* **2016**, *286*, 232–238.
  - (25) Zhao, B.; Zhang, P. Photocatalytic Decomposition of Perfluorooctanoic Acid with β-Ga<sub>2</sub>O<sub>3</sub> Wide Bandgap Photocatalyst. *Catal. Commun.* **2009**, *10* (8), 1184–1187.
  - (26) Li, X.; Zhang, P.; Jin, L.; Shao, T.; Li, Z.; Cao, J. Efficient Photocatalytic Decomposition of Perfluorooctanoic Acid by Indium Oxide and Its Mechanism. *Environ. Sci. Technol.* **2012**, *46* (10), 5528–5534.
  - (27) Jiang, F.; Zhao, H.; Chen, H.; Xu, C.; Chen, J. Enhancement of Photocatalytic Decomposition of Perfluorooctanoic Acid on CeO<sub>2</sub>/In<sub>2</sub>O<sub>3</sub>. *RSC Adv.* **2016**, *6* (76),

- 72015–72021.
- (28) Chen, M. J.; Lo, S. L.; Lee, Y. C.; Huang, C. C. Photocatalytic Decomposition of Perfluorooctanoic Acid by Transition-Metal Modified Titanium Dioxide. *J. Hazard. Mater.* **2015**, *288*, 168–175.
  - (29) Hori, H.; Nagaoka, Y.; Murayama, M.; Kutsuna, S. Efficient Decomposition of Perfluorocarboxylic Acids and Alternative Fluorochemical Surfactants in Hot Water. *Environ. Sci. Technol.* **2008**, *42* (19), 7438–7443.
  - (30) Yamada, T.; Taylor, P. H.; Buck, R. C.; Kaiser, M. A.; Giraud, R. J. Thermal Degradation of Fluorotelomer Treated Articles and Related Materials. *Chemosphere* **2005**, *61* (7), 974–984.
  - (31) Vecitis, C. D.; Wang, Y.; Cheng, J.; Park, H.; Mader, B. T.; Hoffmann, M. R. Sonochemical Degradation of Perfluorooctanesulfonate in Aqueous Film-Forming Foams. *Environ. Sci. Technol.* **2010**, *44* (1), 432–438.
  - (32) Appleman, T. D.; Higgins, C. P.; Quiñones, O.; Vanderford, B. J.; Kolstad, C.; Zeigler-Holady, J. C.; Dickenson, E. R. V. Treatment of Poly- and Perfluoroalkyl Substances in U.S. Full-Scale Water Treatment Systems. *Water Res.* **2014**, *51*, 246–255.
  - (33) McCleaf, P.; Englund, S.; Östlund, A.; Lindegren, K.; Wiberg, K.; Ahrens, L. Removal Efficiency of Multiple Poly- and Perfluoroalkyl Substances (PFASs) in Drinking Water Using Granular Activated Carbon (GAC) and Anion Exchange (AE) Column Tests. *Water Res.* **2017**, *120*, 77–87.
  - (34) Woodard, S.; Berry, J.; Newman, B. Ion Exchange Resin for PFAS Removal and Pilot Test Comparison to GAC. *Remediation* **2017**, *27* (3), 19–27.
  - (35) Pramanik, B. K.; Pramanik, S. K.; Suja, F. A Comparative Study of Coagulation, Granular- and Powdered-Activated Carbon for the Removal of Perfluorooctane Sulfonate and Perfluorooctanoate in Drinking Water Treatment. *Environ. Technol. (United Kingdom)* **2015**, *36* (20), 2610–2617.
  - (36) Franke, V.; McCleaf, P.; Lindegren, K.; Ahrens, L. Efficient Removal of Per- And Polyfluoroalkyl Substances (PFASs) in Drinking Water Treatment: Nanofiltration Combined with Active Carbon or Anion Exchange. *Environ. Sci. Water Res. Technol.* **2019**, *5* (11), 1836–1843.
  - (37) Atkinson, C.; Blake, S.; Hall, T.; Kanda, R.; Paul, R. *Survey of the Prevalence of Perfluorooctane Sulphonate (PFOS), Perfluorooctanoic Acid (PFOA) and Related Compounds in Drinking Water and Their Sources*; 2008.
  - (38) Thompson, J.; Eaglesham, G.; Reungoat, J.; Poussade, Y.; Bartkow, M.; Lawrence, M.; Mueller, J. F. Removal of PFOS, PFOA and Other Perfluoroalkyl Acids at Water Reclamation Plants in South East Queensland Australia. *Chemosphere* **2011**, *82* (1), 9–17.
  - (39) Appleman, T. D.; Dickenson, E. R. V.; Bellona, C.; Higgins, C. P. Nanofiltration and Granular Activated Carbon Treatment of Perfluoroalkyl Acids. *J. Hazard. Mater.* **2013**, *260*, 740–746.
  - (40) Tang, C. Y.; Fu, Q. S.; Criddle, C. S.; Leckie, J. O. Effect of Flux (Transmembrane Pressure) and Membrane Properties on Fouling and Rejection of Reverse Osmosis and

Nanofiltration Membranes Treating Perfluorooctane Sulfonate Containing Wastewater. *Environ. Sci. Technol.* **2007**, *41* (6), 2008–2014.

- (41) Aher, A.; Nickerson, T.; Jordan, C.; Thorpe, F.; Hatakeyama, E.; Ormsbee, L.; Majumder, M.; Bhattacharyya, D. Ion and Organic Transport in Graphene Oxide Membranes: Model Development to Difficult Water Remediation Applications. *J. Memb. Sci.* **2020**, 118024.
- (42) Takagi, S.; Adachi, F.; Miyano, K.; Koizumi, Y.; Tanaka, H.; Mimura, M.; Watanabe, I.; Tanabe, S.; Kannan, K. Perfluorooctanesulfonate and Perfluorooctanoate in Raw and Treated Tap Water from Osaka, Japan. *Chemosphere* **2008**, *72* (10), 1409–1412.
- (43) Quiñones, O.; Snyder, S. A. Occurrence of Perfluoroalkyl Carboxylates and Sulfonates in Drinking Water Utilities and Related Waters from the United States. *Environ. Sci. Technol.* **2009**, *43* (24), 9089–9095.